Numerical characterization of whispering-gallery mode optical microcavities

Zhixiong Guo, Haiyong Quan, and Stanley Pau

We characterize planar microcavities in whispering-gallery mode optical resonances. The microcavity consists of a waveguide and a microdisk, and a nanoscale gap separates the waveguide and the microdisk. The devices can be fabricated on Si-based thin films by using conventional microelectronics techniques. To characterize these types of cavity, we study a broad range of resonator configuration parameters including the size of the microdisk, the width of the gap, and the waveguide dimensions. The finite-element method is used for solving Maxwell's equations. The electric fields and the energy density distributions are obtained and compared between the on-resonance and off-resonance situations. A brilliant ring with a strong electric field and a high-energy density is found inside the periphery of the microdisk under first-order resonance. While under second-order resonance, there are two bright rings, and the light intensity in the inner ring is stronger than that in the outer ring. The resonant frequencies and their free spectral ranges are predominantly determined by the size of the microdisk. The gap effect on the resonant frequencies is observable, although it is minor. The gap strongly affects the full width at half-maximum (FWHM), finesse, and quality factor of the resonances. With an increase in the gap width from 100 to 300 nm, both the Q value and finesse increase substantially, while the FWHM decreases. The waveguide width has a visible influence on the Q value, FWHM, and finesse as well.

OCIS codes: 230.5750, 260.5740, 170.6280, 230.3990, 130.6010.

1. Introduction

Advances in micro- and nanofabrication techniques have made it feasible to consider optical resonators having physical or feature dimensions of the order of one optical wavelength or less. As a particular mode of microcavity resonances,[1] whispering-gallery modes (WGMs) occur at specific wavelengths when light rays travel in a dielectric medium of circular geometry such as spheres, disks, rings, and cylinders. The resonance occurs when the electromagnetic (EM) field closes on itself at the curvilinear boundary after repeated total internal reflections. Since the pioneering work[2] in the excitation of WGM resonances of microspheres on an optical fiber, microcavity WGM resonators have attracted increasing attention in research and technology development in recent years due to their high potentials for realization of microlasers,[3] narrow filters,[4] optical switching,[5] single molecule detection biosensors,[6] and high-resolution spectroscopy.[7]

As stressed by Arnold,[1,8] WGMs are morphology-dependent resonances. The resonant frequencies depend on the size of the resonator. In general, the resonant modes for a circular resonator are approximately predicted by $2\pi rn = mc_0/f$, where m is an integer, n is the refractive index of the cavity material, r is the radius of the cavity, and f is the resonant frequency of mode m. The frequency shift of a given resonant mode is estimated to be $\Delta f/f = -(\Delta r/r + \Delta n/n)$, where Δr and Δn represent small changes of the radius and refractive index of the cavity, respectively. If we assume a constant refractive index and consider the linewidth of the resonance to be the smallest measurable shift (taken as $\Delta f = 10$ MHz, $f = 3.75 \times 10^8$ MHz at $\lambda = 800$ nm), then the smallest "measurable" size change is $|\Delta r|_{\min} = 2.6 \times 10^{-8} r$. With a radius r in the range of 1–10 μm in a typical microcavity, $|\Delta r|_{\min}$ is down to the order of 10^{-4} nm, which is an order of magnitude smaller than the size of an atom that is potentially detectable in theory.

Such a feature is being explored for use as detectors

Z. Guo (guo@jove.rutgers.edu) and H. Quan are with the Department of Mechanical and Aerospace Engineering, Rutgers, the State University of New Jersey, Piscataway, New Jersey 08854. S. Pau is with Nanofabrication Research Laboratory, Lucent Technologies/Bell Labs, Murray Hill, New Jersey 07974.

Received 3 May 2005; accepted 15 July 2005.
0003-6935/06/040611-08$15.00/0

and sensors for identifying molecules surrounding the peripheral surface of WGM resonators. When peptides, protein molecules, or cell membranes are attached on a resonator, for example, they interact with the evanescent radiation field around the resonator. The interactions polarize the molecules or target analytes and change the effective size and/or refractive index of the resonator. All these can lead to a detectable frequency shift in the resonance modes. Thus it is possible to identify and detect single molecules by observing the resonant frequency shifts in WGM-based optical sensors.[8–10] These optical resonance techniques can also be used to enhance the existing sensitivity of biosensor devices.[11,12]

To optimize the sensitivity of specific molecules detection, we must design a cavity configuration with high finesse. Experimental methods for conducting such a task are very time consuming and costly. Analytical models[13] have been introduced to analyze optical resonant phenomena associated with small particles, such as the perturbation model.[14] Analytical solutions are very useful and powerful in understanding the physical essence of the phenomena. Although they can reveal the individual intuitive resonance properties of a microcavity, it is hard for them to capture a completely real picture of a sensor as a system. For example, a perturbation theory is hardly able to account for the coupling of the evanescent fields in the nanoscale gap and the interactions of the resonator with surrounding individual molecules. As a matter of fact, the EM field in the microcavity is very sensitive against the gap through which photons tunnel. A complete modeling of the EM field in the whole WGM structure is highly desired. A flexible numerical characterization can be developed into a practical tool for system and device design and optimization.

Previously, many WGM-based sensors were constructed of a microsphere and an eroded optical fiber coupling structure. Although the Q value for a microsphere-based resonator can be very high, such a configuration may have some flaws for use as an ideal sensor. For instance, mass manufacturing of such devices can be difficult, and nonuniformity exists, especially in the control of the gap distance separating the light-delivery fiber and the resonator. The gap is a critical parameter for photon tunneling and affects the Q value and resonant frequencies, as will be shown in Section 4.

Here we consider sensors of a planar waveguide and microdisk coupling structure. Such devices can be manufactured on silicon-based thin films using conventional silicon integrated circuits (ICs) processing with high uniformity and density. This new cavity structure will further reduce the sensor size and enhance miniaturization of the devices. Planar WGM sensors possess a high sensitivity, a small sample volume, and a robust integrated property for system-on-a-chip applications.

Maxwell's EM theory can be adopted to rigorously describe the radiation–matter interactions in planar WGM microcavities. In this paper, Maxwell's equations are solved using the finite-element method. The characterization of the WGM-based devices is focused on the optical resonant phenomena with respect to a broad range of cavity configuration parameters including the microcavity size, the gap width, and the waveguide width. The effects of these parameters will be scrutinized. The resonant frequencies are chosen in the near infrared range, which is ideal for applications to biomaterials and biomolecules.

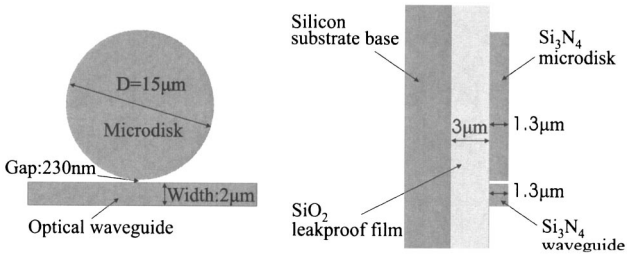

Fig. 1. Sketch of a waveguide–microdisk coupling WGM resonator.

2. Electromagnetic Theory

The sketch of a planar waveguide and microdisk device is shown in Fig. 1. The EM field in the WGM device is governed by time-dependent Maxwell's equations. By introducing time-harmonic waves, the Maxwell's equations can be reduced to two Helmholtz equations as follows:

$$\frac{1}{\mu}\nabla^2\bar{E} + \omega^2\varepsilon_c\bar{E} = 0, \tag{1a}$$

$$\frac{1}{\mu}\nabla^2\bar{H} + \omega^2\varepsilon_c\bar{H} = 0, \tag{1b}$$

where $\bar{E}$ and $\bar{H}$ are the electric and magnetic field vectors, respectively, and $\omega = 2\pi c/\lambda$. We have introduced the complex permittivity $\varepsilon_c = \varepsilon_{cr}\varepsilon_0 = \varepsilon - i(\sigma/\omega)$, where ε_{cr} is the complex relative permittivity and ε_0 is the permittivity in vacuum. ε is the permittivity of the medium, μ is the permeability, and σ is the electrical conductivity. c is the speed of light in the medium and λ is the light wavelength. The relationship between ε_{cr} and m is expressed by[15] $\varepsilon_{cr} = m^2 = n^2 - k^2 - i2nk$. Here the complex index of refraction, $m = n - ik$, is conveniently introduced; n is the real part of the refractive index and represents a spatial phase change of the electromagnetic wave; k is the absorption index and stands for a spatial damping of the electromagnetic wave.

WGM resonance inside the planar microdisk is typically an equatorial brilliant ring, and this ring is located on the same plane as the waveguide. So it is feasible to use a two-dimensional (2D) theoretical model. In the present calculations we apply in-plane TE waves, where the electric field vector has only a z component and it propagates in the x–y plane. Thus the fields can be written as

$$\bar{E}(x,\ y,\ t) = E_z(x,\ y)\bar{e}_z \exp(i\omega t), \tag{2a}$$

$$\bar{H}(x,\ y,\ t) = [H_x(x,\ y)\bar{e}_x + H_y(x,\ y)\bar{e}_y]\exp(i\omega t). \tag{2b}$$

To get a full description of the electromagnetic problem, we also need to specify the boundary conditions. At the interface and physical boundaries, we used the natural continuity condition for the tangential component of the magnetic field:

$$\bar{n} \times \bar{H} = 0. \tag{3}$$

For the outside boundaries, the low-reflecting boundary condition is adopted. The low reflection means that only a small part of the wave is reflected, and that the wave propagates through the boundary almost as if it were not present. This condition can be formalized as

$$\bar{e}_z \cdot \bar{n} \times \sqrt{\mu}\bar{H} + \sqrt{\varepsilon}E_z = 0. \tag{4}$$

The laser excitation source E_{0z}, which propagates inwards through the entry boundary of the waveguide, can be treated as a low-reflecting boundary condition and can be expressed by

$$E_{0z} = \frac{1}{2\sqrt{\varepsilon}}(\bar{e}_z \cdot \bar{n} \times \sqrt{\mu}\bar{H} + \sqrt{\varepsilon}E_z). \tag{5}$$

The WGM resonances have high-quality factors due to minimal reflection losses. The quality factor Q is defined as a ratio of 2π stored energy to energy lost per cycle. From the energy conservation and resonance properties, we can deduce a simple approximate expression[16]:

$$Q = \omega_0/\Delta\omega = 2\pi\omega_0\tau, \tag{6}$$

where ω_0 is the resonant frequency, $\Delta\omega$ is the resonance linewidth, and τ is the photon lifetime.

To find the radiation energy conservation, Poynting's theorem[17] is employed:

$$\oint_S (\bar{E} \times \bar{H}) \cdot \bar{n}\,\mathrm{d}S = -\int_V \left(\bar{E} \cdot \frac{\partial \bar{D}}{\partial t} + \bar{H} \cdot \frac{\partial \bar{B}}{\partial t}\right) dV - \int_V \bar{J} \cdot \bar{E}\,\mathrm{d}V, \tag{7}$$

where V is the computation element volume and S is the closed boundary surface area of V. The term on the left-hand side of Eq. (7) represents the radiative losses. The quantity $\bar{S} = \bar{E} \times \bar{H}$ is called as the Poynting vector. The first integral on the right-hand side represents the rate of change in total energy. The second integral on the right-hand side represents the resistive losses that result from heat dissipation in metallic materials. For dielectric materials with negligible absorption index, we assume zero electric current density, i.e., $\bar{J} = 0$. Thus the change in total energy of the EM field is totally converted to radiative energy.

3. Simulation Model

More than 30 years ago, Silvester[18] developed high-order Lagrange elements and first applied the finite-element method (FEM) for solving EM field problems. Recently, Quan and Guo[10] successfully applied the FEM to simulate the EM and radiation energy fields in the WGM resonators of a microsphere and an optical fiber coupling structure. Although the finite-difference time-domain (FDTD) method[19] has been commonly adopted in computational electrodynamics, the FEM has advantages in terms of the treatment of irregular configurations. This is very useful for simulation-based optimal design purposes.

In the present computations, the FEM is employed for solving the Helmholtz equations. Detailed description of the solution scheme has been given in a recent paper,[10] and thus is not repeated here. FEMLAB is used for finite-element analysis and pre- and post-processing.

Silicon nitride (Si_3N_4) is selected as the material for the waveguide and microdisk because this substance has excellent physical and thermal stability, low cost, and extremely low optical absorption around the operating wavelengths.[20,21] The thickness of the Si_3N_4 thin film is 1.3 μm. A 3 μm thick layer of SiO_2 is employed as the low cladding of the device. These thin films can be deposited on the surface of silicon wafer by using low-pressure chemical-vapor deposition or plasma-enhanced chemical-vapor deposition. The large refractive index of Si_3N_4 ensures high contrast of refractive indices between the WGM resonator and its surrounding medium (gas phase or aqueous solutions) and can result in high-quality resonance modes. Figure 2 shows scanning electron microscopy (SEM) photos of a fabricated such device using 248 nm optical lithography and silicon IC processing.

A typical simulation domain is a 20 μm $\times$ 25 μm rectangular area with a centered microdisk (as the cavity) and a waveguide (for light delivery) below the microdisk. The microdisk and waveguide are separated by a small gap. The length of the waveguide is extended to the edge of the simulation domain. A laser beam from a tunable continuous-wave (CW) laser is coupled into the left end of the waveguide to excite the resonance. The frequency of the incident laser varies between 364 THz (824 nm) and 376 THz (798 nm). When the frequency of the input light is the same as a natural resonant frequency of the cavity, the WGM is excited. At the resonant frequency, the scattering intensity from the microdisk will increase sharply and form a peak in the intensity–frequency spectrum.

The computational domain is meshed by 51,400 triangle elements. Since fine meshes are required in

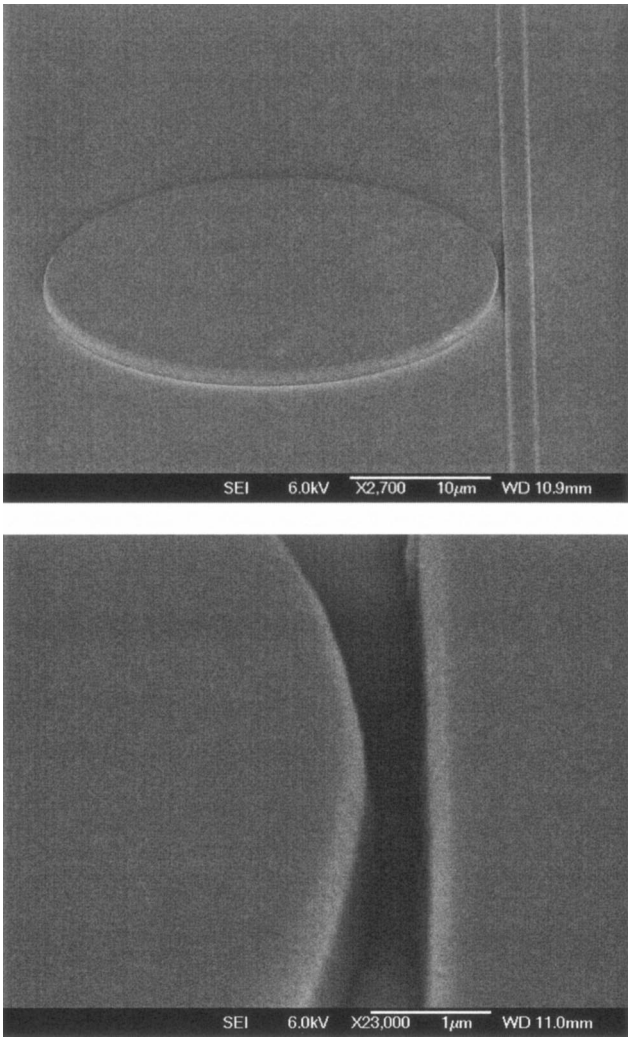

Fig. 2. SEM photos of a fabricated WGM microcavity.

the vicinity around the periphery of the cavity, hierarchical meshing is employed to scale the cavity down to two different spatial levels (this is why a solid internal circle is observed in Figs. 3 and 4 in Section 4). The general computational resolution of the excitation wavelength is 0.5 nm, but special attention is paid to the resonance frequency vicinities where 0.01 nm resolution is adopted. To conduct parametric studies, the diameter of the microdisk varies between 10 and 15 μm. The width of the waveguide changes between 2 and 3 μm. The gap distance between the microdisk and waveguide varies between 100 and 300 nm.

4. Results and Discussion

First we investigate the EM fields and radiation energy distributions under WGM resonances and off resonance, respectively, and observe the differences under various operation conditions. Figures 3 and 4 exhibit the distributions of the electric field and the radiation energy density, respectively, for three different operating conditions. Comparisons can be performed between the off resonance, the first-order resonance, and the second-order resonance. The first- and second-order resonance frequencies are found at 373.78 THz ($\lambda = 802.61$ nm) and 372.96 THz (804.37 nm), respectively. The off-resonance frequency is selected at 372.67 THz ($\lambda = 805.00$ nm). The diameter of the microdisk is 15 μm and the surrounding medium is air. The gap width, which is defined as the smallest distance between the waveguide and microdisk, is $g = 230$ nm and the width of the waveguide is $w = 2$ μm. The refractive index of the cavity and waveguide material is assumed to be constant at 2.01 at the operating wavelengths.[21] These general parametric values are used throughout the paper unless otherwise specified.

In Fig. 3 we see that the EM field exists in the microdisk even when resonant phenomenon does not occur. Photons tunnel from the waveguide to the microdisk because the gap width is less than one optical wavelength. For the first-order resonance, we see a buildup of EM field forming inside the microdisk in the vicinity close to the peripheral surface. The strength of the electric field in the ring is stronger than that in the waveguide through where the excitation light is delivered. While in the case of the second-order resonance, there are two bright rings inside the microdisk. The strength of the EM field in the inner ring is stronger than that in the outer ring. Under the off-resonance condition, however, the EM field is confined in the waveguide and its strength in the cavity is very weak.

From Fig. 4 it is seen that the microdisk and waveguide coupling resonator has an appealing property of high-energy storage in the cavity when WGMs occur. The majority of the energy stores in the thin ring inside the peripheral surface of the microdisk

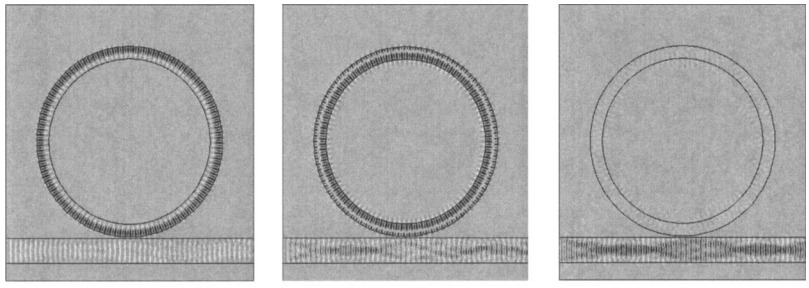

Fig. 3. Electric fields under (a) the first-order resonance, (b) the second-order resonance, and (c) off resonance.

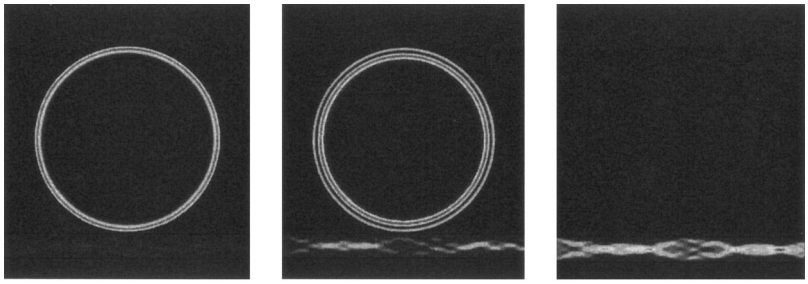

Fig. 4. Energy distributions under (a) the first-order resonance, (b) the second-order resonance, and (c) off resonance.

under first-order resonance. For second-order resonance, the energy is stored in two rings and the light intensity in the inner ring is stronger. The ratio of the radiation energy storing in the microdisk to the energy passing through the waveguide is found to be 10.5 for the first-order resonance, whereas this ratio is only 0.008 for the off-resonance case. The increase of energy storage in the small volume cavity leads to enormous enhancement of the micro- and nanoscale radiation fields around the periphery of the resonator, which can potentially be used to sense any external perturbation.

Figure 5 shows the scattering spectra for three different microdisk diameters: $d = 10, 12.5$, and 15 μm, respectively. Three first-order resonant frequencies (modes) are found for each of the microdisk sizes in the frequency range considered (364–376 THz). We find that the microdisk size affects significantly the resonant frequencies and their intervals. The free spectral range (FSR), which represents the periodicity of resonance peaks, increases with the decreasing diameter of the microdisk. The FSR of the resonant modes is 3.273 ± 0.007 THz for the case of $d = 15$ μm, 3.940 ± 0.009 THz for the case of $d = 12.5$ μm, and 4.954 ± 0.010 THz for the case of $d = 10$ μm. Such wide FSRs make the WGM microcavities excellent candidates for detection and distinguishing of trace gas and molecules using the spectroscopy method.

To scrutinize the effects of cavity configurations, the resonance data retrieved from the scattering spectra in Fig. 5 are listed in Table 1. The resonance data include the resonant frequency and its corresponding wavelength, the quality factor, the full width at half-maximum (FWHM) of the resonant frequency band, the FSR, and the finesse of the resonant mode defined by F = FSR/FWHM. To inspect the effects of gap width and waveguide width, we obtain the scattering spectra for three different gap widths ($g = 100, 200$, and 300 nm, respectively) and three different waveguide widths ($w = 2.0, 2.5$, and 3.0 μm, respectively). These are also listed in Table 1.

From Table 1 it is clear that the resonant frequencies are predominantly determined by the size of the microdisk. The gap width also affects the resonant frequencies although its effect is in a finite range of 0.1 THz (of the order of 0.1 nm in terms of wavelength) for the four different gap widths considered. Such an effect can be attributed to the gap influence on the orientation of photon tunneling. The influencing range of the waveguide on the resonant frequencies for the waveguide widths considered is not more than 0.01 THz, which is almost comparable to the computation resolution. Thus the waveguide width may have negligible effect on the resonant frequencies.

The path length of the m-mode resonant photons orbiting the periphery of the cavity is estimated to be approximately $2mr \sin(\pi/m)$. Thus the resonant frequencies can be analytically approximated as

$$f = \frac{c_0}{2rn \sin(\pi/m)}. \tag{8}$$

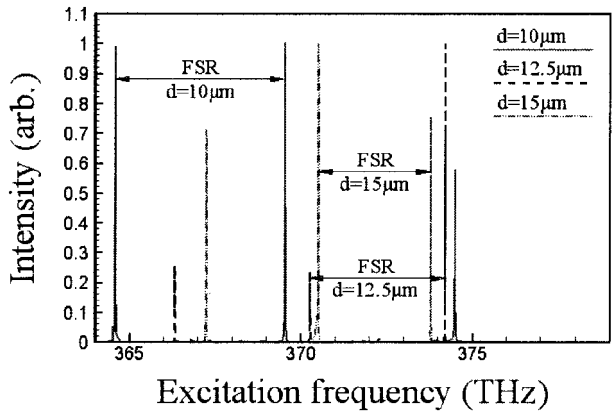

Fig. 5. Scattering spectra for different microdisk sizes of $d = 10, 12.5$, and 15 μm, respectively.

The analytically estimated frequencies using Eq. (8) are compared with the numerically predicted frequencies in Fig. 6. Although the two methods give consistent results, it is seen that the difference of the resonant frequencies between the two methods could be as large as 1 THz. Nevertheless, Eq. (8) is simple and can give a reasonable estimation of the resonant frequencies.

Figure 7 further portrays the gap effects on the quality factor Q and finesse F of the resonances. Four different gap widths of 100, 200, 230, and 300 nm are selected for comparison. Since there are three resonant modes in the frequency range considered, three sets of Q values and two sets of FSR data are obtained

Table 1. Resonance Data From the Scattering Spectra

Resonance Frequency (THz)	Excitation Wavelength (nm)	Quality Factor Q	FWHM (THz)	FSR (THz)	Finesse F
Case 1: $d = 10.0$ μm, $g = 230$ nm, $w = 2.0$ μm					
364.582	822.86	21,446	0.017	4.944	282.5
369.526	811.85	20,529	0.018		
374.490	801.09	22,029	0.017	4.964	283.6
Case 2: $d = 12.5$ μm, $g = 230$ nm, $w = 2.0$ μm					
366.321	818.53	22,895	0.016	3.931	253.6
370.252	810.26	24,683	0.015		
374.201	801.71	22,011	0.017	3.949	246.8
Case 3: $d = 15.0$ μm, $g = 230$ nm, $w = 2.0$ μm					
367.235	816.92	21,602	0.017	3.266	210.7
370.501	809.72	26,464	0.014		
373.780	802.61	23,361	0.016	3.279	218.6
Case 4: $d = 15.0$ μm, $g = 100$ nm, $w = 2.0$ μm					
367.197	817.00	10,200	0.036	3.267	92.0
370.464	809.79	10,585	0.035		
373.743	802.69	12,056	0.031	3.279	99.4
Case 5: $d = 15.0$ μm, $g = 200$ nm, $w = 2.0$ μm					
367.224	816.94	19,328	0.019	3.267	186.7
370.495	809.73	23,155	0.016		
373.776	802.63	21,987	0.017	3.281	198.8
Case 6: $d = 15.0$ μm, $g = 300$ nm, $w = 2.0$ μm					
367.235	816.91	183,617	0.002	3.275	1,637.5
370.510	809.70	185,255	0.002		
373.791	802.59	124,597	0.003	3.281	1,312.4
Case 7: $d = 15.0$ μm, $g = 200$ nm, $w = 2.5$ μm					
367.215	816.96	26,230	0.014	3.277	211.4
370.492	809.73	21,794	0.017		
373.765	802.64	23,360	0.016	3.273	198.4
Case 8: $d = 15.0$ μm, $g = 200$ nm, $w = 3.0$ μm					
367.217	816.96	40,802	0.009	3.271	344.3
370.488	809.74	37,049	0.010		
373.764	802.65	46,721	0.008	3.276	364.0

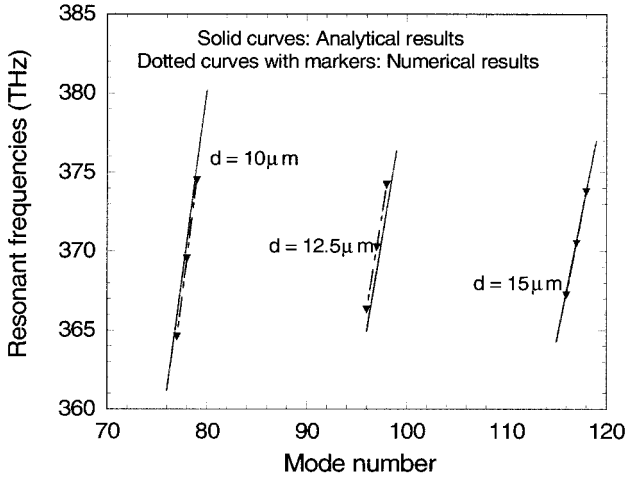

Fig. 6. Comparisons between analytically estimated resonant frequencies and numerically predicted resonant frequencies.

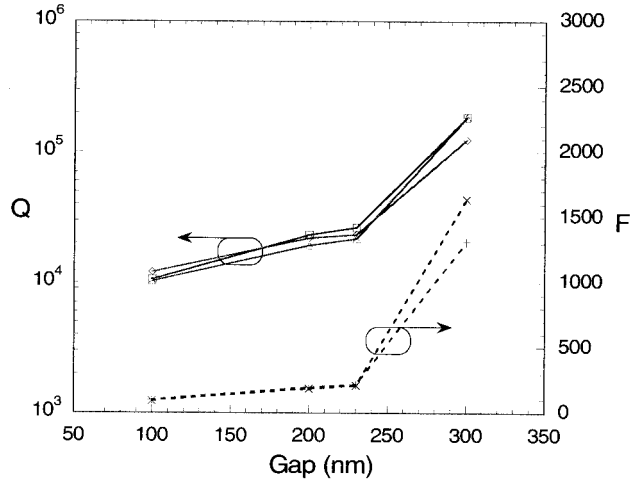

Fig. 7. Effects of the gap on the resonant quality factor Q and finesse F.

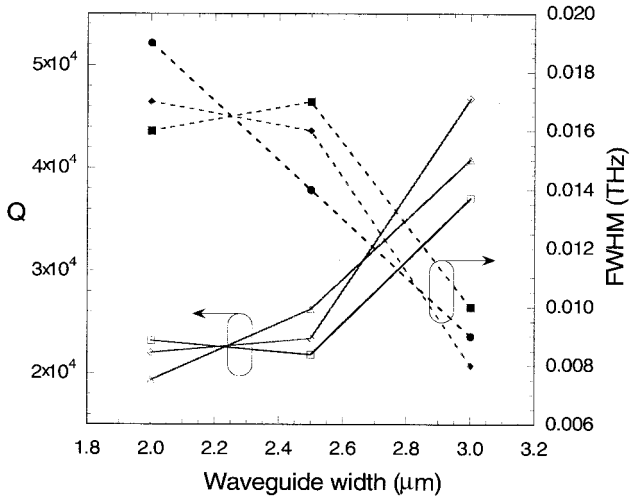

Fig. 8. Effects of the waveguide width on the resonant quality factor Q and FWHM.

and displayed. With the increase of the gap width from 100 to 300 nm, it is seen that both the Q and F values increase by over an order of magnitude. Examining Table 1, it is found that the gap width does not obviously affect the FSR, but does strongly influence the FWHM of the resonant bands. The larger the gap width, the narrower the FWHM. In terms of the quality factor and FWHM, the effect of the microdisk size is very slight.

The effects of the waveguide width on the Q value and the FWHM are shown in Fig. 8 for the three resonant modes. With the decrease in the waveguide width, the FWHM of the resonance generally increases, but the Q value decreases. From Table 1 it is obvious that the waveguide width does not influence the FSR. Comparing Figs. 7 and 8, we see that the value of the gap has a much larger effect on the resonance than the value of the waveguide width. In this paper, we have just selected several typical values for the gap width. Since the gap could be designed to up to one optical wavelength or down to zero (when the resonator and waveguide are in close contact), a more detailed scrutiny of the gap effect in a wider spectrum of the gap width is needed and will be the focus of our next report.

5. Conclusions

The characteristics of planar WGM microcavities with a waveguide–microdisk coupling structure were investigated numerically. The EM fields and radiation energy distributions in the devices were obtained through the solution of Maxwell's equations. It was found that photon tunneling between the waveguide and microdisk is very weak under the off-resonance condition and the radiation energy is well confined inside the waveguide. When WGM resonance occurs, photon tunneling is greatly enhanced and significant radiation energy is stored in the microcavity. A very brilliant ring with a strong EM field and a high radiation intensity exists inside the periphery of the microdisk under first-order resonance, whereas there are two bright rings inside the cavity under the second-order resonance, the strength of the outer ring is weaker than that of the inner ring. Thus the first-order resonances may be preferred in sensing applications because the interactions of interest occur in the evanescent field surrounding the cavity periphery. The WGM resonant frequencies are predominantly determined by the size of the cavity. The gap separating the waveguide and the cavity has also influence on the resonant frequencies. But the waveguide size has negligible effect on the resonant frequencies. The Q value is substantially influenced by the gap width. The difference in Q values between 100 and 300 nm gaps is over 1 order of magnitude. The waveguide width also affects the Q value. Increasing the waveguide width will increase the Q value. The FSR of the resonances reaches to several THz for the considered WGM microcavities. It is mainly decided by the size of the cavity and little affected by the gap and waveguide widths. The FWHM of the resonances is strongly influenced by the gap width. A wider gap results in a narrower FWHM. The increase of the waveguide width leads to the reduction of the FWHM. The finesse of the resonances is affected by the gap and waveguide widths and the size of the cavity. Among these parameters, the gap width influences the finesse the most. With an increase of the gap width from 100 to 300 nm, the F value increases substantially. The finesse also increases as the cavity size decreases or the waveguide width increases.

Z. Guo acknowledges the partial support of the Academic Excellence Fund Award from Rutgers University, the New Jersey Nanotechnology Consortium, and a National Science Foundation grant (CTS-0318001) to the project.

References

1. S. Arnold, "Microspheres, photonic atoms and the physics of nothing," Am. Sci. **89,** 414–421 (2001).
2. A. Serpenguzel, S. Arnold, and G. Griffel, "Excitation of resonances of microspheres on an optical fiber," Opt. Lett. **20,** 654–656 (1995).
3. M. Cai, Q. Painter, K. J. Vahala, and P. C. Sercel, "Fiber-coupled microsphere laser," Opt. Lett. **25,** 1430–1432 (2000).
4. B. E. Little, S. T. Chu, H. A. Haus, J. Foresi, and J. P. Laine, "Microring resonator channel dropping filters," J. Lightwave Technol. **15,** 998–1005 (1997).
5. F. C. Blom, D. R. van Dijk, H. J. Hoekstra, A. Driessen, and T. J. A. Popma, "Experimental study of integrated-optics micro-cavity resonators: Toward an all-optical switching device," Appl. Phys. Lett. **71,** 747–749 (1997).
6. R. W. Boyd and J. E. Heebner, "Sensitive disk resonator photonic biosensor," Appl. Opt. **40,** 5742–5747 (2001).
7. S. Schiller and R. L. Byer, "High-resolution spectroscope of whispering gallery modes in large dielectric spheres," Opt. Lett. **16,** 1138–1140 (1991).
8. S. Arnold, M. Khoshsima, I. Teraoka, and F. Vollmer, "Shift of

whispering-gallery modes in microspheres by protein adsorption," Opt. Lett. **28,** 272–274 (2003).
9. F. Vollmer, D. Braun, A. Libchaber, M. Khoshsima, I. Teraoka, and S. Arnold, "Protein detection by optical shift of a resonant microcavity," Appl. Phys. Lett. **80,** 4057–4059 (2002).
10. H. Quan and Z. Guo, "Simulation of whispering-gallery-mode resonance shifts for optical miniature biosensors," J. Quant. Spectrosc. Radiat. Transfer **93,** 231–243 (2005).
11. S. Blair and Y. Chen, "Resonant-enhanced evanescent-wave fluorescence biosensing with cylindrical optical cavities," Appl. Opt. **40,** 570–582 (2001).
12. R. W. Boyd and J. E. Heebner, "Sensitive disk resonator photonic biosensor," Appl. Opt. **40,** 5742–5747 (2001).
13. P. W. Barber and P. K. Chang, *Optical Effects Associated with Small Particles* (World Scientific, 1988).
14. I. Teraoka, S. Arnold, and F. Vollmer, "Perturbation approach to resonance shifts of whispering-gallery modes in a dielectric microsphere as probe of a surrounding medium," J. Opt. Soc. Am. B **20,** 1937–1946 (2003).
15. M. F. Modest, *Radiative Heat Transfer,* 2nd ed. (Academic, 2003).
16. A. Yariv, *Optical Electronics in Modern Communications,* 5th ed. (Oxford University Press, 1997).
17. A. Kovetz, *The Principles of Electromagnetic Theory* (Cambridge U. Press, 1990).
18. P. P. Silvester, "Finite element solution of homogeneous waveguide problems," Alta Freq. **38,** 313–317 (1969).
19. A. Taflove and S. C. Hagness, *Computational Electrodynamics: The Finite-Difference Time-Domain Method,* 2nd ed. (Artech House, 2000).
20. T. R. Hsu, *MEMS & Microsystems Design and Manufacture* (McGraw-Hill, 2002).
21. E. D. Palik, *Handbook of Optical Constants of Solids* (Academic, 1985).